International Journal of
Geo-Engineering

ORIGINAL RESEARCH

Open Access

Monotonic and dynamic properties of riverbed sand and hill-slope soils of seismically active North-east India for ground engineering applications

Shiv Shankar Kumar[1*], Arindam Dey[2] and A. Murali Krishna[3]

*Correspondence:
shivshankar.mit@gmail.com;
k.shiv.ce@nitp.ac.in
[1] Department of Civil
Engineering, National
Institute of Technology Patna,
Bihar 800005, India
Full list of author information
is available at the end of the
article

Abstract

The stress–strain characteristics of soil under monotonic loading conditions and the dynamic properties of soils under cyclic loading are necessary for foundation engineering, ground response analysis and soil structure interaction studies. In the absence of site/region-specific properties, it is a common practice to use representative parameters based on the index properties of soil and available standard correlations. Such correlations might be inadequate for regional soils of varying index properties. Based on monotonic and cyclic triaxial tests, this study reports the monotonic and dynamic soil properties of the prevalent soils from the northeastern region of India, namely the cohesionless, cohesive and silty-sandy soils. It is observed that monotonic response of cohesionless soil is mostly influenced by the initial relative density, while the response of cohesive and silty-sands are primarily influenced by the effective confining pressure and degree of saturation. The cyclic triaxial tests revealed that, irrespective of the soil type, the strain-dependent modulus reduction and especially the damping ratio curves are noticeably different from available standards. The study highlights the importance of identifying the site/region specific soil properties for their usage in GRA and SSI applications.

Keywords: Cohesionless and cohesive soil, Silty-sand, Relative density, Shear strain, Degree of saturation, Staged loading, Shear stiffness, Modulus reduction, Damping ratio
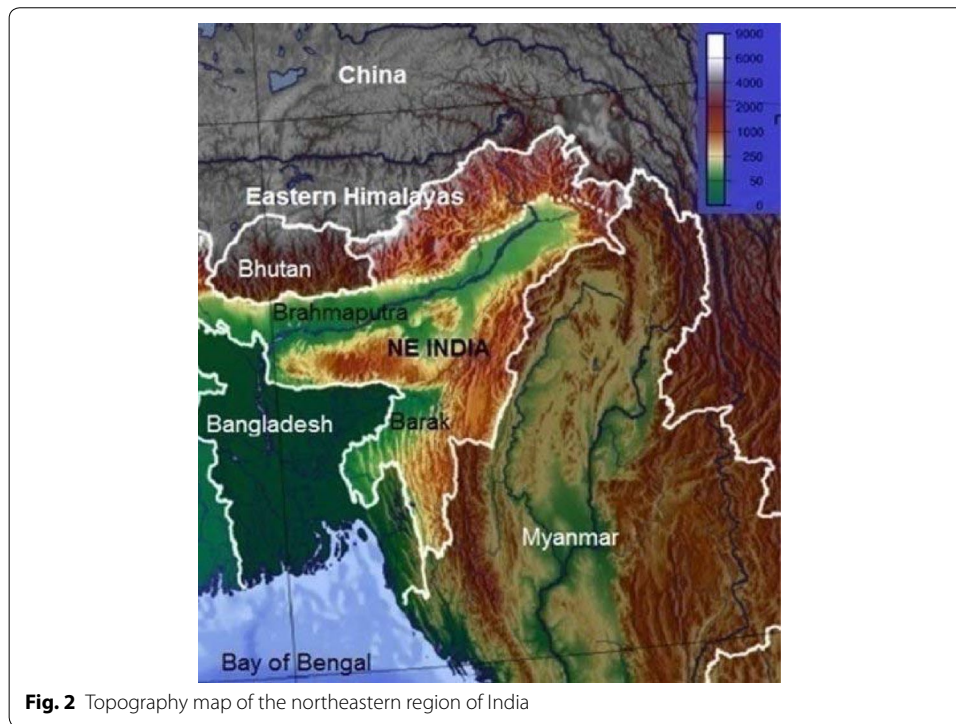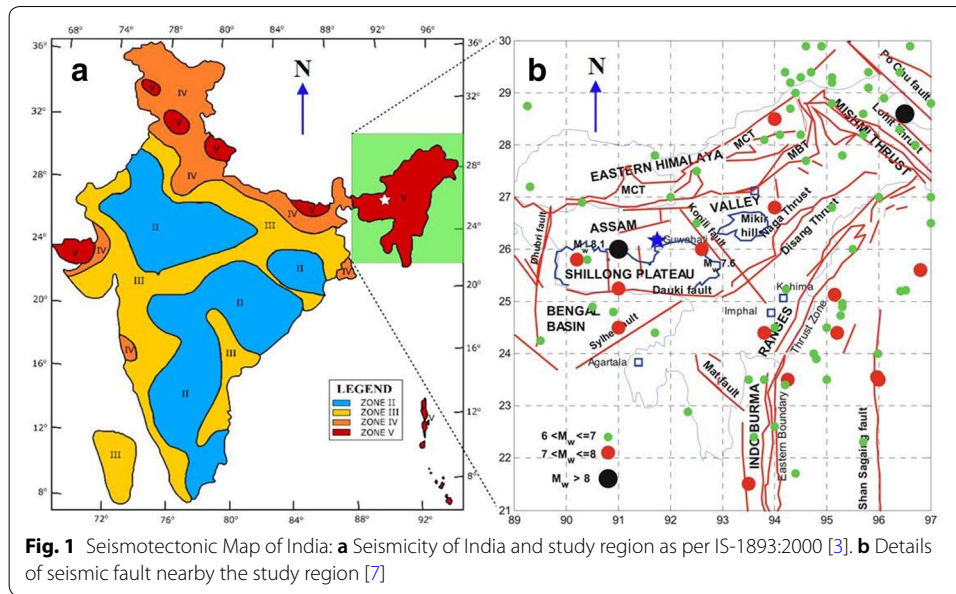
Introduction

Monotonic and dynamic soil properties are extremely important parameters for any ground engineering applications such as soil-structure interaction, foundation engineering, slope stability and seismic ground response analyses. The mechanical behaviour of soils is primarily a manifestation of the strain- or stress-dependent soil parameters, namely the Young modulus (E), Poisson's ratio (ν), cohesion (c), friction angle (ϕ), dilatancy angle (ϕ), shear stiffness (G), and shear strain (γ), to name a few. These fundamental soil parameters can be evaluated from different laboratory experimentation procedures such as oedometer tests, triaxial tests, direct shear tests, and other forms

of advanced strength and compressibility tests. The above-stated parameters, or their variants, form the skeleton of various types of constitutive models (Linear elastic model, Mohr–Coulomb model, Hardening soil model, Soft-soil model, Cam-clay model and others) that are commonly used in several commercial software such as PLAXIS, FLAC, ABAQUS and Rocscience. There are several instances where the absence of realistic site-specific material properties, the researchers are prompted to utilize the standard data available in existing literatures and adopt a presumptive model for the soil response. Such adoption might be incorrect in many instances, mostly when the site specific material does not exhibit a conformity to the soil based on which the standard model was developed by earlier researchers.

The dynamic response of soil and soil-supported structures during earthquake is primarily influenced by the soil stratification, strain-dependent stiffness and damping of the soil, and the amplitude and frequency content of the incumbent earthquake motions [1]. It is very important to conduct a proper ground response analysis when a new structure is to be built on a seismically active region. Such studies aid in the understanding of seismic soil-structure interaction (SSSI), and discover how the seismically driven subsoil would affect the natural and forced response of the building. At the same time, it is also important to conduct a seismic requalification study of the earlier existing structures, in order to account for the temporal change in tectonic conditions as well as the temporal degradation of the structural characteristics. Such requalification studies are now common, as has been carried out by Dammala et al. [2] for one of the very important road bridges in North-east India, i.e. the 1,492 km long Saraighat Bridge on River Brahmaputra that was constructed during 1959–1962. The importance of the study is immense since this bridge was constructed at a time when the seismic design codes were either non-existent, or not prevalent. As per IS 1893, the Northeast region of India comes under Seismic Zone V [3]. Earlier researchers have reported that this region has experienced several earthquakes of moderate to large magnitude [4–7]. Since the literatures and studies on the monotonic and dynamic response of soils of the Northeast (NE) region are scanty [8–10], it is required to have a detailed monotonic and dynamic characterization of the soils prevalent in this region for better understanding of the soil behaviour and ensuring better serviceability of structures. Kumar et al. [11] have highlighted the importance of region-specific dynamic soil properties for earthquake resistant design and their consideration in round response analysis (GRA) using standard commercial software namely SHAKE2000 [12], DEEPSOIL [13] and PLAXIS [14]. Based on the varying origin, the NE region of India consists of different type of soils such as sand, clay, silt, silty-sand and in their various mix proportions. Based on the robust experimental investigations, this paper presents the monotonic and dynamic response of various soils (cohesionless soil, cohesive soil and silty-sand) of Northeast region, India, which can be suitably used for various ground engineering applications.

Seismicity of Northeast India for the importance of present study

Based on the past earthquake data, tectonic setup and geology, the Northeast India comprises six seismic blocks i.e. Shillong Plateau, Assam Valley, Eastern Himalaya, Mishmi Thrust, Bengal Basin and Indo-Burmese range presented in Fig. 1 [3, 7, 15]. The topography of this region consists of several hills and isolated hillocks made of

Fig. 1 Seismotectonic Map of India: **a** Seismicity of India and study region as per IS-1893:2000 [3]. **b** Details of seismic fault nearby the study region [7]

Fig. 2 Topography map of the northeastern region of India

Precambrian granitic rocks with varying altitude from 50 to 60 m above mean sea level (MSL), as shown in Fig. 2. Almost all northeastern states have experienced several devastating earthquakes of different magnitudes ranging from M_w 5–8.7. According to the Indian seismic code [3], the entire northeastern region comes under one of the most seismically active region in the world. Poddar [5] and Raghukanth [6] have reported that Assam experienced massive liquefaction, approximately in 126 acres

area, during the 1950 Assam earthquake. Thus, keeping in view of the prevalent seismicity, scenario of the past earthquakes, and scarcity of the monotonic and dynamic behaviour of soils of this region, the results presented in this study will be of immense importance for ground engineering applications for the Northeast region of India.

Materials

Three type of soils namely cohesionless soil (i.e. Brahmaputra riverbed sand, or BS), cohesive soil (Red soil, or RS) and silty-sand soil (or SS), collected from Guwahati region, Assam (India), have been used in this study. Figure 3 exhibits two borehole profiles highlighting the typical stratification and existence of various prevalent soils in the northeastern region of India. Each soils have different physical property, thereby ensuing their variations with each other. The following sections elaborates the three types of soils chosen for the present study.

Cohesionless soil

The particle size distribution of cohesionless soil, determined by conducting sieve analysis [16], is presented in Fig. 4. It is clearly observed that the soil conforms to the range of fine sand and can be classified as poorly graded sand (SP), as per the relevant standards [17]. The index properties of the soil such as the specific gravity and the dry unit weights were determined as per relevant standards [18, 19], and are presented in Table 1.
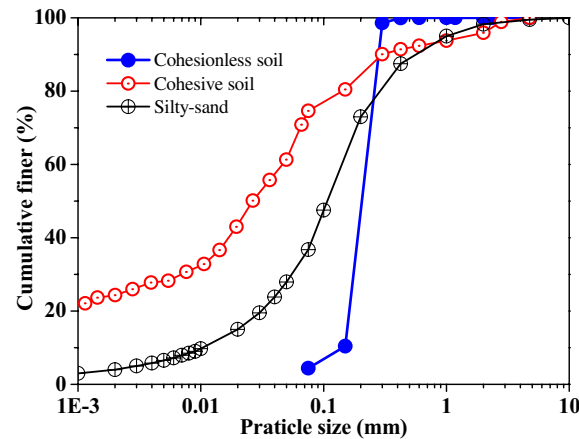

Fig. 3 Typical borehole stratigraphy and prevalent soils of northeastern region of India
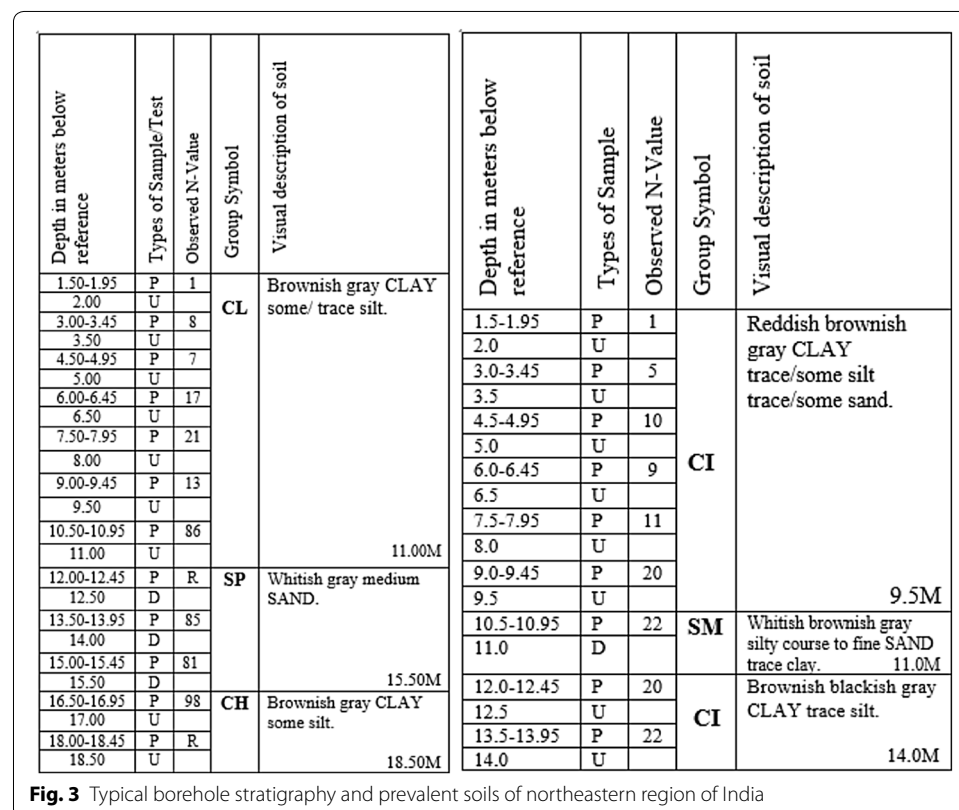
Fig. 4 Particle size distribution of the soils used in the present study

Table 1 Physical properties of the soils used in the present study

Physical properties	Sandy soil	Cohesive soil	Silty-sand
Specific gravity (G_s)	2.70	2.65	2.68
Liquid limit (LL, %)	–	41.5	35
Plastic limit (PL, %)	–	22.6	Non-plastic
Plasticity index (PI, %)	–	18.9	–
Uniformity coefficient, C_u	1.47	–	2.63
Coefficient of curvature, C_c	1.09	–	1.08
Maximum unit weight ($\gamma_{d,max}$, kN/m³)	16.84	–	–
Minimum unit weight ($\gamma_{d,min}$, kN/m³)	13.85	–	–
Maximum dry density (MDD, g/cm³)	–	1.75	1.57
Optimum moisture content (OMC, %)	–	19.3	15.3

Cohesive soil

The particle size distribution of the cohesive soil obtained from wet sieving [20] as well as hydrometer analysis [21], representing 21.23% clay (less than 0.002 mm), 48.50% silt (0.002 mm–0.075 mm), and 30.27% fine sand (0.075 mm–4.75 mm), is presented in Fig. 4. The other relevant index properties of the soil namely the specific gravity, Atterberg limits, plasticity index, and compaction characteristics, are determined by the methodologies described in relevant standards [22–24], and are summarised in Table 1. As per Unified Soil Classification System [17], the soil is classified as low-plastic cohesive soil (CL).

Silty-sand soil

This soil is collected from the hill-slope of Guwahati region (Assam, India). The particle size distribution for the collected samples, as obtained from standard laboratory investigation [21], is highlighted in Fig. 4; while, the index properties are summarized in Table 1. As per Unified Soil Classification System [17], the soil is classified as silty sands or sand-silt mixture (SM).

Experimental procedure: apparatus, sample preparation and experimental program
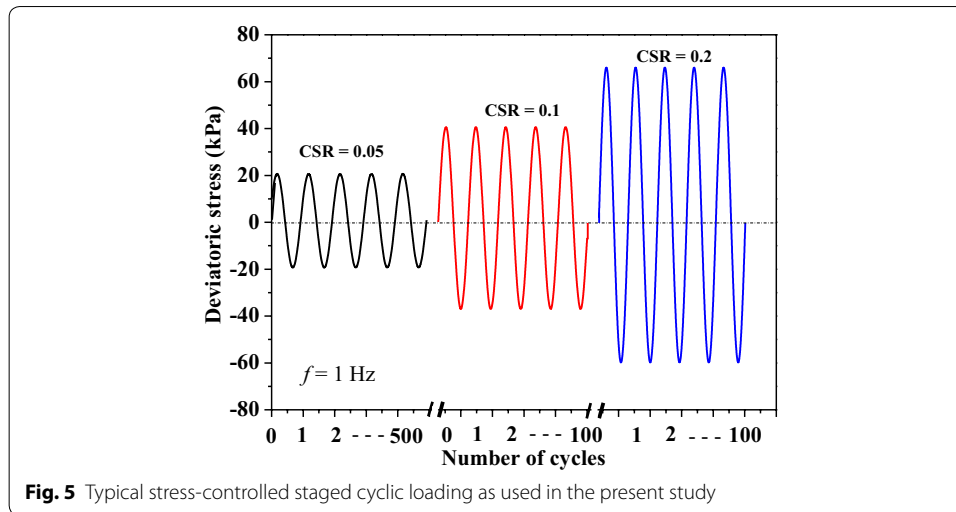
Cyclic triaxial apparatus, which facilitates both monotonic as well as cyclic test, was used for the experimental investigations. The details of instrumentations available with the apparatus are described in Kumar et al. [9]. All the tests were conducted on the remoulded cylindrical soil specimens of dimensions 70 mm diameter and 140 mm height [25]. The preparation of cohesionless and cohesive soil specimens are discussed in detail in Kumar et al. [9, 26] and Kumar et al. [27], respectively. For cohesionless soil, dry pluviation technique was adopted to prepare the soil specimens. Each of the samples was prepared in three layers. Dry sand was poured through a cone shaped funnel into the sample-forming mould. A vacuum pressure of 15–20 kPa was applied before removing the mould to maintain the verticality of the specimen. Subsequently, the triaxial cell was mounted on the base plate supporting the test specimen. The cell was then filled with water, followed by simultaneous application of cell pressure and release of vacuum pressure. The applied maximum cell pressure was so maintained that the specimen was still supported by a pressure of 15–20 kPa at the time when all the vacuum pressure was released. In order to prepare the cohesive and silty-sand soil specimen, similar methods as reported in Kumar et al. [27] were used. For the cohesive soil and silty-sand soil specimens, dry soil of a specified weight was firstly mixed with the required amount of water. Once the water was uniformly mixed with the soil, the entire quantity of water-mixed soil was transferred into the mould from one end, while other end was maintained fixed with the collar. Thereafter, compaction was done from both ends by giving simultaneous equal rotation to the collars, maintaining uniformity of the specimen, till the specimen length of 140 mm was obtained. The specimen prepared in mould was extracted with the aid of an extruder. Thereafter, the extracted soil specimen was placed on the base of triaxial cell and supported with a rubber membrane. Subsequently, the triaxial cell was mounted on the base plate and then filled with de-aired water. Thereafter, the specimen was subjected to subsequent saturation and consolidation stages. In order to expedite the saturation process, the specimen was flushed with CO_2 (for 20 min to 1 h, depending on the types of soils) and subsequently, de-aired water was passed through CO_2 flushed specimen. Then, the cell pressure (CP) and back pressure (BP) were sequentially applied to the soil specimen, with a continuous monitoring of the pore-water pressure. The specimen was considered to be completely saturated when the Skempton's *B*-value attained a magnitude greater than 0.96. After saturation, the specimen was isotropically consolidated to a targeted effective confining pressure (σ'_c– 50, 100, 150 and 200 kPa) by increasing the CP while maintaining a constant BP. The consolidated specimens were then subjected to cyclic loading at different investigating parameters, as mentioned in Table 2. The silty-sand specimens (SS1, SS2 and SS3) were prepared at MDD and OMC, as shown in Table 2. The consolidated specimens were then subjected to stress-controlled staged-cyclic loading with sinusoidal waveform of frequency (*f*) 1 Hz (Fig. 5) for evaluating the shear modulus and damping ratio. Kumar et al. [27] and Yoshida [28] have also reported the importance of staged loading in comparison to a single-stage strain-controlled test.

Staged-cyclic loading is a type of stress-controlled loading in which incremental deviatoric stress, with specific number of cycles, is sequentially applied on a single soil

Table 2 Investigating parameters for cohesionless, cohesive and silty-sand soils for the evaluation of dynamic soil properties

Soils	Relative density D_r (%)	Effective confining pressure σ'_c (kPa)	Loading frequency f (Hz)	Axial strain γ (%)
BS Cohesion-less soil	30	50	1	0.015, 0.045, 0.075, 0.15, 0.30,0.45,0.60, 0.75, 1.0, 1.5, 3.0
		100		0.045, 0.075, 0.15, 0.30,0.45,0.60, 0.75, 1.5
		150		0.045, 0.075, 0.15, 0.30, 0.45, 0.60, 0.75
	60	50		0.15, 0.60, 1.0, 1.5, 3.0, 4.5
		100		
		150		
	90	50		0.045, 0.075, 0.15, 0.30, 0.45, 0.60, 0.75, 1.5
		100		0.045, 0.075, 0.15, 0.30, 0.45, 0.60, 1.0, 1.5, 2.0
		150		0.045, 0.075, 0.15, 0.30, 0.45, 0.60, 0.75, 1.0, 1.5, 2.0

Specimen	MDD (g/cm³)	OMC (%)	σ'_c (kPa)	Cyclic Stress Ratio CSR	Number of cycles N_c
RS Cohesive soil					
RS1	1.75	19.3	100±2	0.1	2000
RS2	1.75	19.3	100±2	0.1-0.2-0.3	1060-570-37
RS3	1.75	19.3	100±2	0.2-0.3-0.4	2000-100-24
RS4	1.50	8	100±2	0.1-0.2	500-45
RS5	1.50	8	100±2	0.2	38
RS6	1.50	15	100±2	0.2	32
RS7	1.50	25	100±2	0.2-0.3	123-20
RS9	1.50	8	50±2	0.1-0.2-0.3	500-100-50
SS Silty-sand					
SS1	1.57	15	50	0.05, 0.1, 0.2	500, 100, 100
SS2	1.57	15	100	0.05, 0.1, 0.2	500, 100, 100
SS3	1.57	15	200	0.05, 0.1, 0.2	500, 100, 100

specimen. This type of loading represents the same soil experiencing different stress levels during a single earthquake event comprising foreshocks and the main shock having different stress intensity and magnitude. Such a loading represent a more realistic approach to evaluate the dynamic response of a soil subjected to seismic excitation. Therefore, the stress-controlled staged-loading is a good choice, where continuous tests on a single test specimen provides the dynamic properties of the soil at various strain levels. As already mentioned, the staged cyclic loading represents the foreshocks and subsequent main shocks of the possible seismic motion. In general, the foreshocks of the seismic motion comprise many cycles of low amplitude, followed by subsequent rise in seismic amplitude but accompanied by lesser number of cycles. In the same notion,
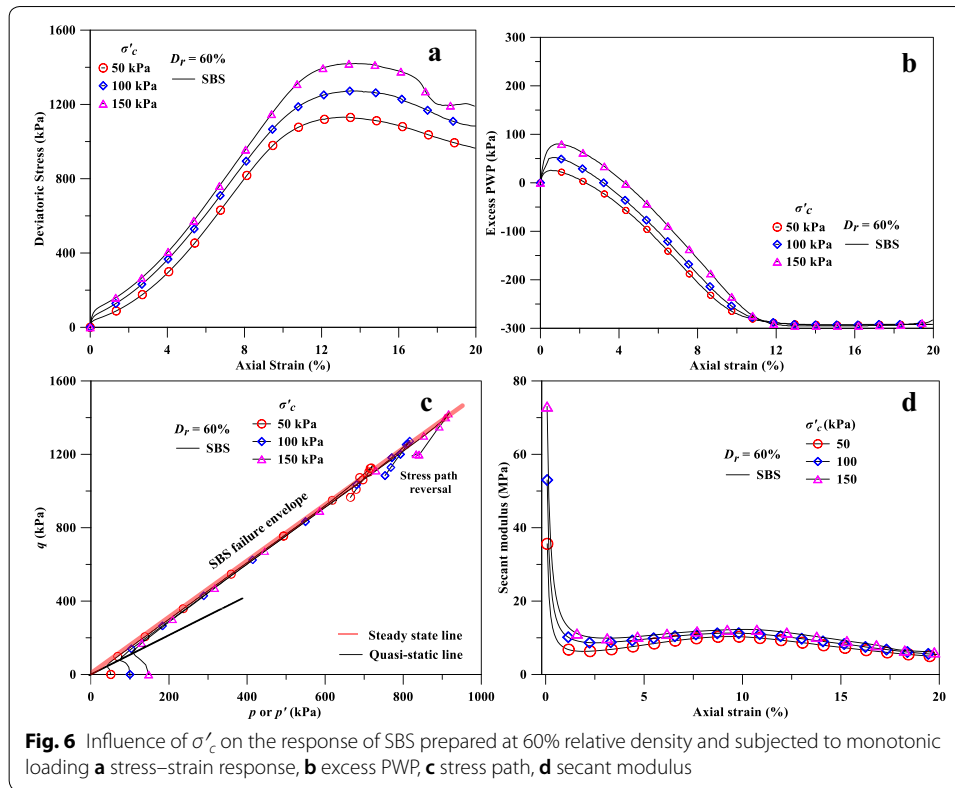
Kumar *et al. Geo-Engineering* (2020) 11:9

Page 8 of 21

Fig. 5 Typical stress-controlled staged cyclic loading as used in the present study

the stress-controlled testing parameters are hypothetically chosen for present study. In this type of loading, the cyclic stress ratio (CSR $= \sigma_d/2\sigma'_c$) is pre-decided for conducting the test, and the deviatoric stress (σ_d) is estimated based on the chosen confining stress (σ'_c). The estimated deviatoric stress of various magnitudes are sequentially employed on the specimen with varying number of cycles to represent the approximate foreshock and mainshock of the seismic motion. For example, in Fig. 4, *CSR* $= 0.05$ represents σ_d on the specimens due to the initial foreshock (provided for 500 cycles), followed by another foreshock of higher σ_d (corresponding to CSR $= 0.1$) applied for 100 cycles. Finally, the main shock, represented by σ_d corresponding to *CSR* $= 0.2$, is applied for 100 cycles. The number of cycles can be suitable altered for a specific test as required.

Results and discussions

Monotonic properties of soils

Cohesionless BS soil

Brahmaputra riverbed sand at saturated conditions (SBS) were tested under monotonic loading to observe the behavioural changes during shearing. To observe the effect of confining pressure, specimens prepared at relative density (D_r) 60% were tested under three different effective confining pressures ($\sigma'_c = 50$ kPa, 100 kPa and 150 kPa). The samples were subjected to monotonic displacement rate of 1.2 mm/min. Figure 6 depicts the influence of effective confining pressure on the overall response of SBS subjected to monotonic loading. Figure 6a illustrates that the strength of the soil (i.e. resistance to deformation) increases with the increase of confining pressure. The maximum deviatoric stress ($\sigma_{d,max}$) attained by SBS specimens for all three σ'_c was found at an axial strain of 14%. It is observed that as compared to the response of specimen at σ'_c 100 kPa, $\sigma_{d,max}$ obtained at 50 kPa is approximately 16% lesser whereas the same obtained at 150 kPa is nearly 8% higher (Fig. 6a). Figure 6b illustrates that with the increase of confining pressure, the excess pore water pressure (PWP) reasonably increases. The increase in excess PWP, up to an axial strain of ~ 1%, in saturated sands subjected to undrained monotonic loading, leads to strength reduction. Such phenomenon in loose sandy soils might lead to the possibility of static liquefaction if there is a significant rise in the excess PWP

Fig. 6 Influence of σ'_c on the response of SBS prepared at 60% relative density and subjected to monotonic loading **a** stress–strain response, **b** excess PWP, **c** stress path, **d** secant modulus

[29–31]. Further straining is responsible for the strength gain due to decrease in excess PWP, thereby indicating soil-dilation with gradual redistribution of PWP within the soil specimen. Since a residual amount of air persists in the specimen at the end of saturation [32], the shearing under undrained conditions shows decrease in excess PWP resulting an increase in degree of desaturation and matric suction [33]. Figure 6c presents the stress-path followed by SBS during shearing, which portrays a higher initial contractive behaviour of sand tested at higher σ'_c. The contractive behaviour of sand, along with the excess PWP development, is more prominent at higher σ'_c. Similar response was obtained by Ishihara [34] for sand prepared at $D_r = 64\%$ and tested under $\sigma'_c = 60$ kPa, 1000 kPa and 3000 kPa, respectively. Further increase in static loading causes increase in effective stress due to the decrease in excess PWP (as shown in Fig. 6b). The strain-dependent secant modulus of SBS is presented in Fig. 6d, which shows that the initial secant modulus is higher at higher σ'_c. However, with the increase in the loading (or axial strain), the secant modulus reduces and marginal difference is observed between the secant moduli at various σ'_c.

To emphasize the effect of D_r on the monotonic response of SBS subjected to $\sigma'_c = 100$ kPa, the tests were conducted at four different D_r (10%, 30%, 60% and 90%), and the outcomes are presented in Fig. 7a–e. Figure 7a depicts the stress–strain response which portrays increase in $\sigma_{d,max}$ at failure with the increase in D_r. It is also observed that D_r has a significant influence on the strain level at which $\sigma_{d,max}$ occurs. At the given $\sigma'_c = 100$ kPa, the increase in $\sigma_{d,max}$ is noted to be approximately 90% for the increase in D_r from 10 to 60%, whereas the increase of the former is nearly 17% for the increase
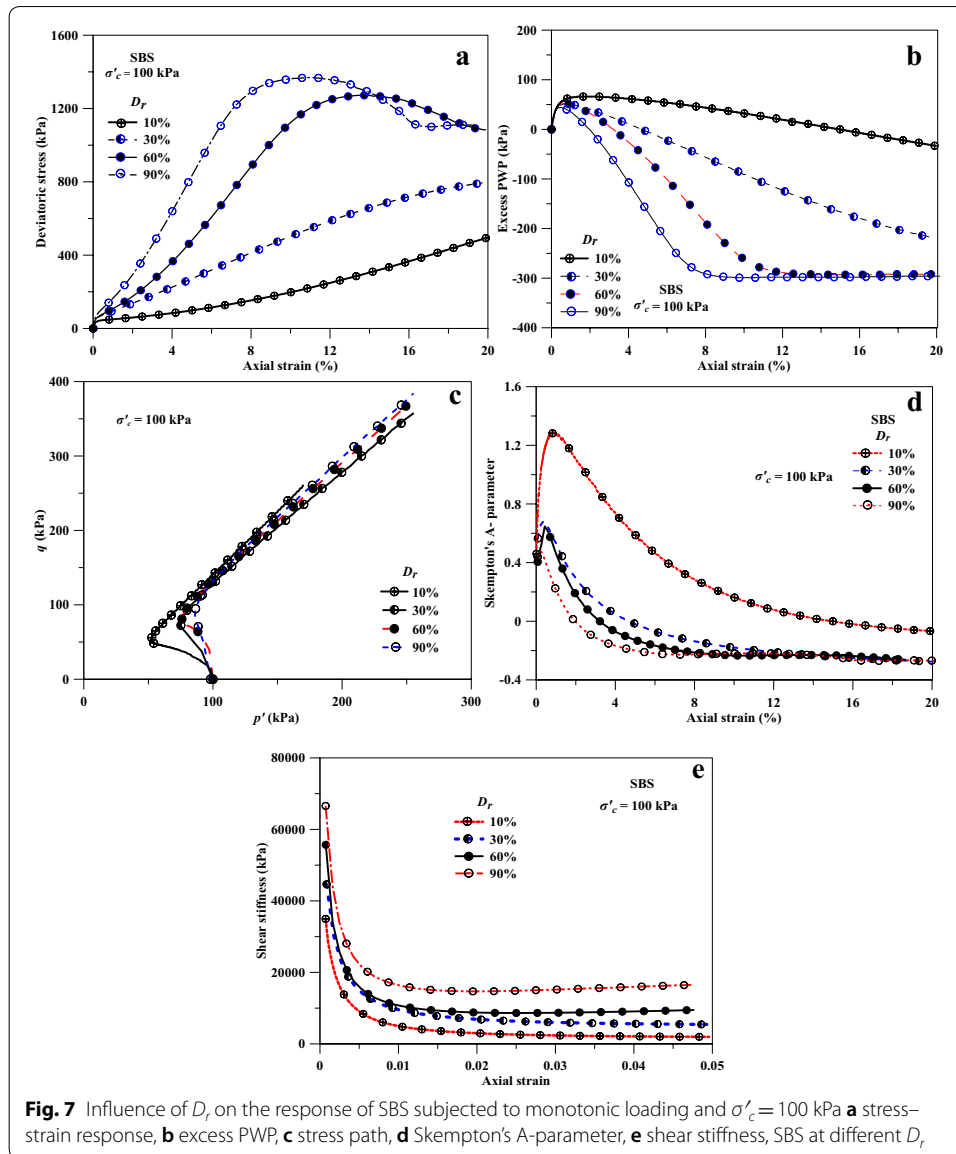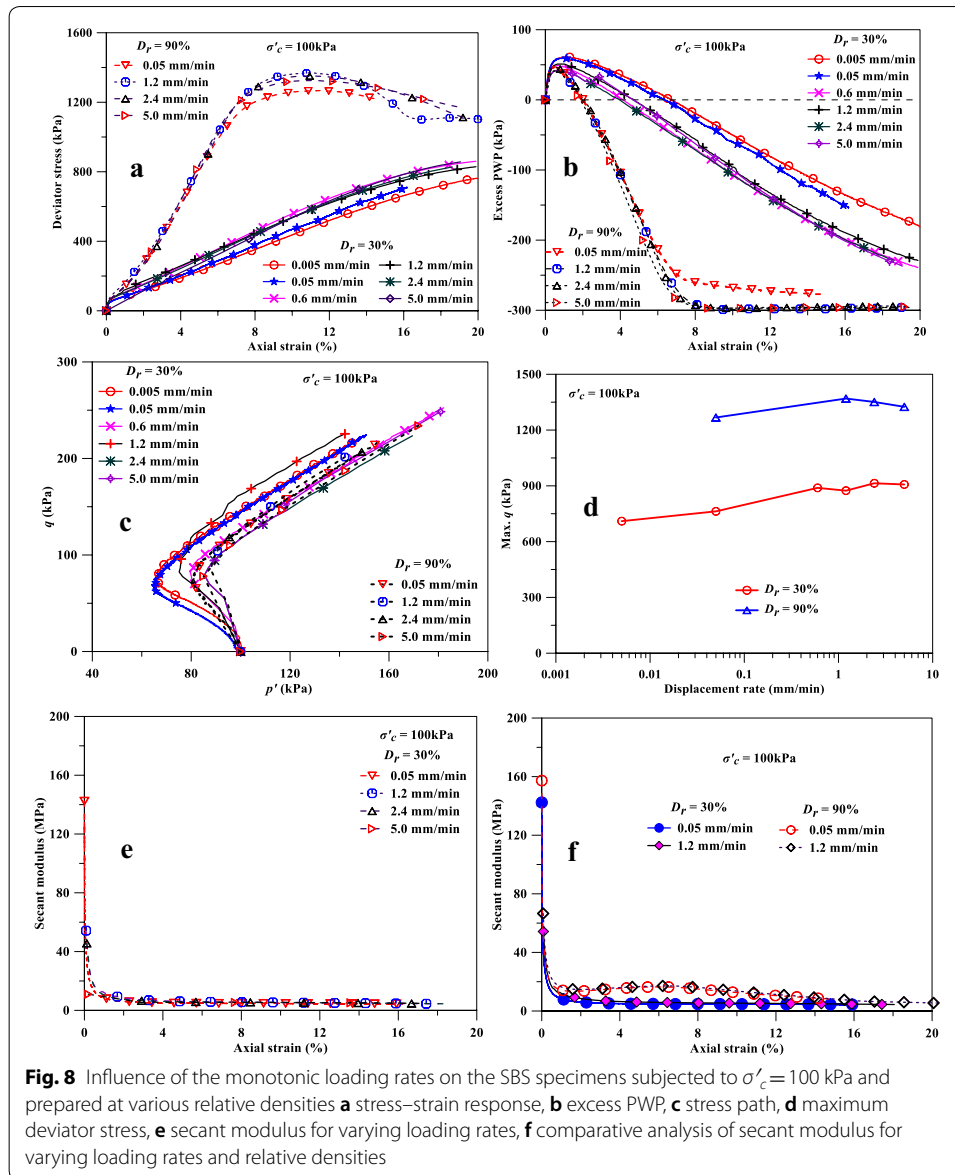
Fig. 7 Influence of D_r on the response of SBS subjected to monotonic loading and $\sigma'_c = 100$ kPa **a** stress–strain response, **b** excess PWP, **c** stress path, **d** Skempton's A-parameter, **e** shear stiffness, SBS at different D_r

in D_r from 60 to 90%. Hence, it can be stated that the effect of D_r is more prominent in the range of loose-to-medium dense sands. Figure 7b illustrates the influence of D_r on the excess PWP generated at varying axial strains. It can be observed that for all the specimens prepared at different D_r, the rate of increase in excess PWP is nearly same up 0.5% axial strain. However, further increase in loading reflects the influence of relative density on the decrement of excess PWP, wherein it is observed that the rate of decrease in excess PWP increases with increase in relative density. From Fig. 7b, it can also be reported that even if the specimen is prepared at $D_r = 30\%$, it does not behave like loose soil, as indicated by the development of negative PWP. Similar response was observed by Ishihara [34] for sand specimens prepared at $D_r = 16\%$ and 38%. Figure 7c presents the effective stress path for SBS prepared at different D_r. It reflects that the effective stress path becomes nonlinear at its yield point due to the nonlinear increase in the excess
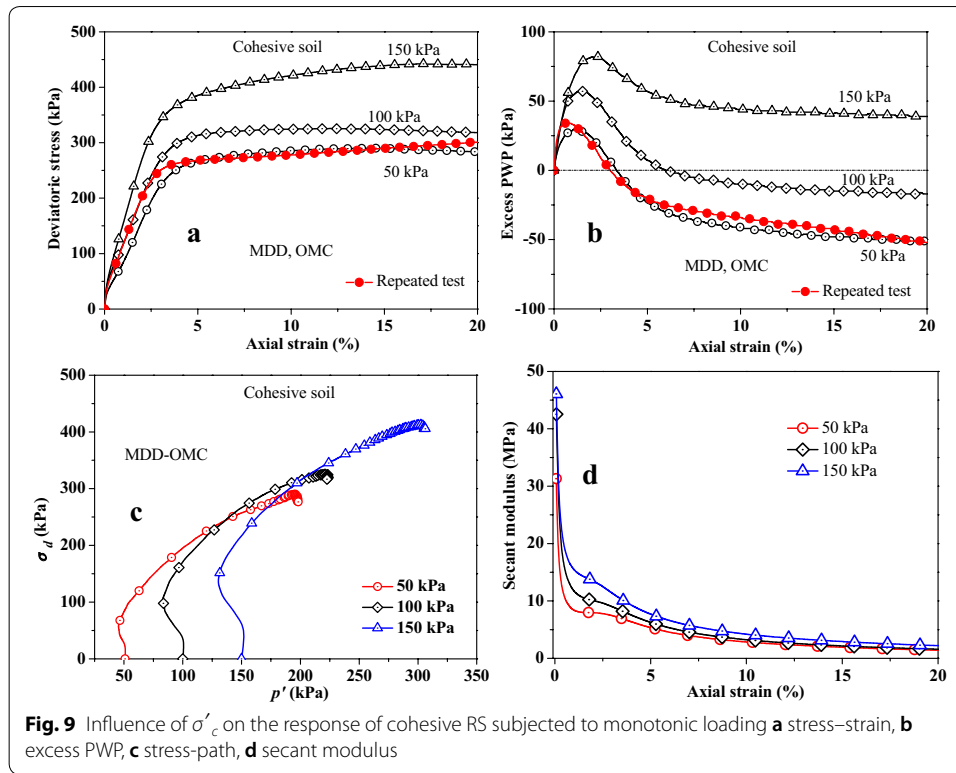
Fig. 8 Influence of the monotonic loading rates on the SBS specimens subjected to $\sigma'_c = 100$ kPa and prepared at various relative densities **a** stress–strain response, **b** excess PWP, **c** stress path, **d** maximum deviator stress, **e** secant modulus for varying loading rates, **f** comparative analysis of secant modulus for varying loading rates and relative densities

PWP under monotonic loading, resulting in the concavity in effective stress path [35]. Figure 7d shows that D_r significantly influences Skempton's A-parameter at the initial stages of loading, while the influence substantially reduces at higher strains, more so for the samples prepared at higher relative densities. Figure 7e highlights the considerable influence of relative density of the prepared specimen on the strain-dependent secant modulus.

Monotonic shear tests were also performed on SBS specimens (reconstituted at $D_r = 30\%$, 60% and 90%, and $\sigma'_c = 100$ kPa) at different loading rates ranging between 0.005 and 5.0 mm/min. Figure 8a highlights the stress–strain response of SBS prepare at $D_r = 30\%$ and 90%. It can be observed that the strength increases with the increase of loading rate up to 0.6 mm/min and 1.2 mm/min for $D_r = 30\%$ and 90% respectively, beyond which the effect is minimal. It can also be noted that with the increase of D_r
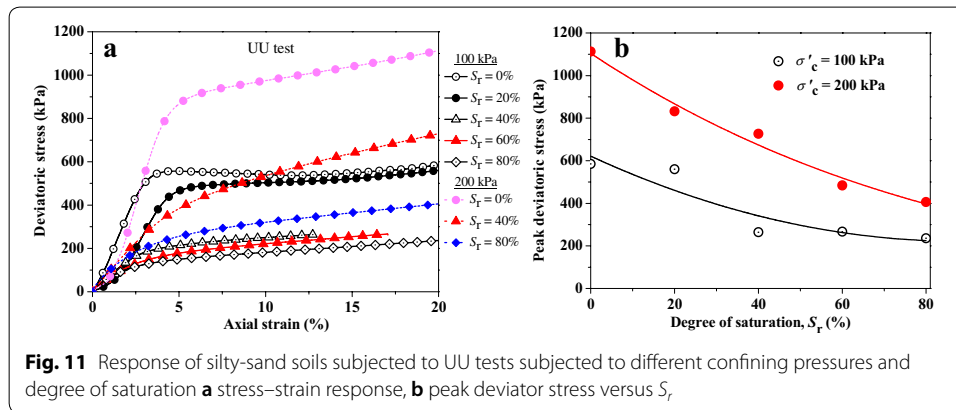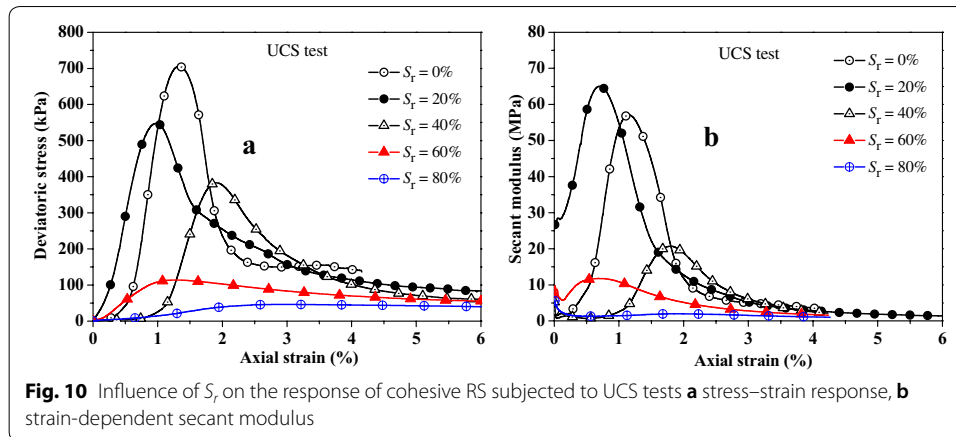
from 30 to 90%, $\sigma_{d,max}$ at failure increased by nearly 75% while the axial strain reduced by approximately 50%. It can be stated that with the increase in D_r (from loose to very dense), the ductility of the soil gets partially compensated, since the higher interlocking of the particles at high D_r generates higher angle of internal friction (ϕ) and higher shear strength. Figure 8b reflects the rise and redistribution of excess PWP during undrained monotonic compression tests at $D_r = 30\%$ and 90%. It is observed that at $D_r = 30\%$, the rise of PWP in the specimen subjected to loading rate of 0.005 mm/min is higher than when subjected to 5.0 mm/min, and the redistribution of excess PWP is lesser at 0.005 mm/min. The rise and redistribution of excess PWP in specimens prepared at $D_r = 90\%$ was not found to be affected by loading rate. It can be observed from effective stress path plot (Fig. 8c) that the specimens shows more initial compression at slower displacement rate. Corresponding to specimen prepared at $D_r = 30\%$, Fig. 8d illustrates that $\sigma_{d,max}$ increases by approximately 25% with the increase of loading rate up to 0.6 mm/min, beyond which the increment is minimal ($\sim 2\%$). Similarly, for samples prepared at $D_r = 90\%$, $\sigma_{d,max}$ increases approximately by 9% with the increase of loading rate up to 1.2 mm/min, beyond which a negligible decrement is noted. The strain-dependent secant modulus at two different relative densities ($D_r = 30\%$ and 90%) for different loading rates are presented in Figs. 8e and 6f, respectively. From Fig. 8e, it can be observed that the secant modulus of saturated sand decreases with the increase of loading rates up to approximately 1% strain levels, beyond which the influence of loading rate diminishes significantly. Figure 8f reveals that the secant modulus of SBS, although being influenced by D_r, remains substantially unaffected by loading rates at higher strains.

Cohesive RS soil

Figure 9 represents the influence of σ'_c on the response of the cohesive RS subjected to consolidated undrained (CU) monotonic triaxial tests. Figure 9a presents the variation in the stress–strain response of RS subjected to varying σ'_c (50 kPa, 100 kPa and 150 kPa). It can be observed that similar to BS, an increase in σ'_c results in the increase in stiffness, thereby manifesting steeper slope in the plot. In order to ensure the accuracy of the results, the tests with $\sigma'_c = 50$ kPa were repeated, wherein the outcomes exhibited a meagre difference of nearly 5%. It is found that for all the cases, $\sigma_{d,max}$ is attained at axial strain of approximately 20%, using which the peak friction angle (ϕ) and cohesion for RS were found to be in the range of 22º–25º and 70–80 kPa, respectively. Figure 9b presents the variations of excess PWP in the cohesive soil specimens subjected to different σ'_c. It can be observed that the excess PWP increases up to axial strain of 2%, beyond which it decreases and becomes negative for higher confining pressures ($\sigma'_c = 50$ kPa and 100 kPa). This observation is attributed to the overconsolidated behaviour of soil, since the cohesive soil (Red Soil, i.e. RS) specimens were prepared at MDD-OMC condition. Figure 9c presents the influence of σ'_c on the stress-path plots of cohesive RS soil. For all the cases, it can be noted that the mean effective stress (p') reduces for the initial part of the test, thereby highlighting contractive response of the soil; whereas, beyond $p' = 45$, 82 and 130 kPa (for $\sigma'_c = 50$, 100 and 150 kPa, respectively), the dilating nature of RS is manifested. Figure 9d represents the variations in secant modulus with axial strains, which is similar to that reported in Fig. 6d; in this case as well, except for the initial axial strains, the variation in σ'_c do not significantly influence the outcome.

Fig. 9 Influence of σ'_c on the response of cohesive RS subjected to monotonic loading **a** stress–strain, **b** excess PWP, **c** stress-path, **d** secant modulus
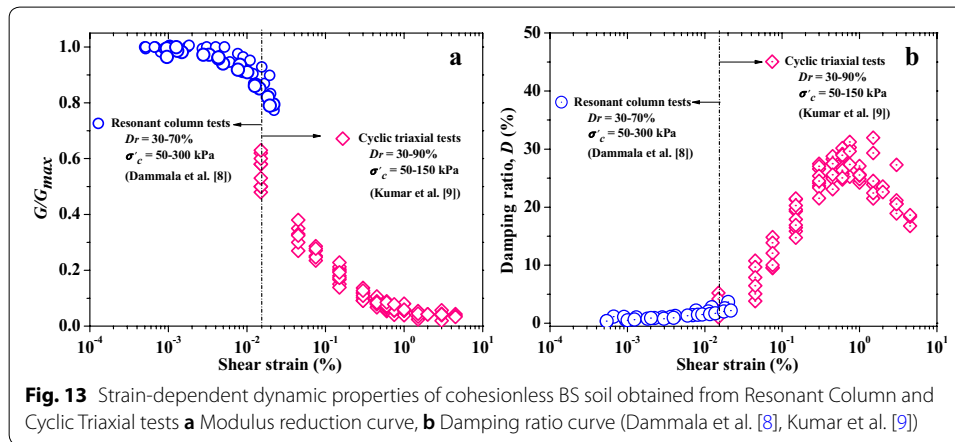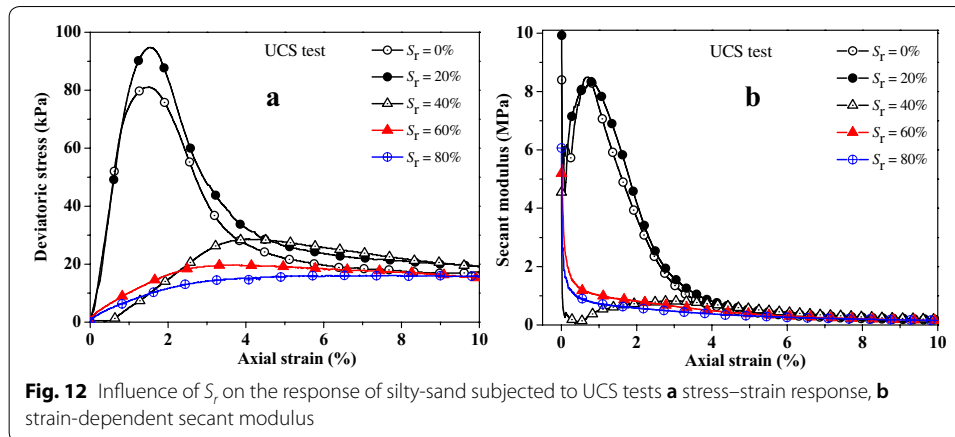
Unconfined compression strength (UCS) tests were also carried out on cohesive RS soil specimens prepared at different degrees of saturation (S_r chosen in the range of 0–80%). UCS test is one of the quick methods to measure the shear strength of soil. Although this test is inappropriate for friable clays that fall apart without any lateral confinement, the RS soil shows its own capacity to stand vertically without any lateral support. Nevertheless, the tests were carried out at $S_r=0$ with the aid of a thin rubber membrane. However, for $S_r>0$, the soil specimens were prepared in such a way that the dry density of the soil specimen turns out to be approximately 1.57 g/cm^3, while the water content is varied so that the specimens attain the desired S_r. The applied load was gradually increased to shear the sample, while the resulting deformation was recorded. The loading was continued until the soil developed an obvious shearing plane or attained excessive deformations. The recorded data were then used to identify the stress–strain characteristics and the strength of the soil. The maximum load per unit area is defined as the unconfined compressive strength, q_u. Figure 10a illustrates that with the increase in degree of saturation (i.e. from $S_r=0\%$ to 80%), as expected, the compressive strength of soils decreased. This is attributed to the loss of friction between the soil particles with the addition of water while the higher levels of saturation were targeted. Figure 10b presents the variations in secant modulus with axial strain for different S_r, which also reflects the variations in soil stiffness. It can also be noted, as expected, that the soil stiffness is almost negligible at very high magnitude of S_r.

Kumar *et al. Geo-Engineering*   (2020) 11:9

Page 14 of 21

Fig. 10 Influence of S_r on the response of cohesive RS subjected to UCS tests **a** stress–strain response, **b** strain-dependent secant modulus

Fig. 11 Response of silty-sand soils subjected to UU tests subjected to different confining pressures and degree of saturation **a** stress–strain response, **b** peak deviator stress versus S_r

Silty-sand SS soil

Figure 11 presents the behaviour of silty-sand soil prepared at different S_r and subjected to unconsolidated undrained (UU) triaxial tests. Figure 11a illustrates the stress–strain response of specimens prepared at $S_r = 0–80\%$ and subjected to $\sigma'_c = 100$ and 200 kPa. With the increase in the degree of saturation, significant decrease in the stress–strain characteristics can be noted, along with the decrement in the peak strength or the peak deviatoric stress (Fig. 11b). As obvious, the peak deviatoric stress of SS soil is found to be higher when the specimen is subjected to higher σ'_c.

Unconfined compression strength (UCS) tests were also performed on the silty-sand soil prepared at different S_r and the results are presented in Fig. 12. The soil being silty-sand, it is very difficult to make the specimens for UCS tests at dry as well as saturated conditions. Hence, to maintain the verticality of the specimens, a thin rubber membrane was used. Figure 12a illustrates the stress–strain response of specimens prepared at $S_r = 0\%$ to 80%, wherein the reduction in the stress–strain can be well recognized with the increase in the degree of saturation of the specimen. As expected, the peak deviatoric stress obtained from UCS tests (Fig. 12a) is observed to be significantly lesser than the same obtained from UU tests (Fig. 11a). Figure 12b shows the variations in secant modulus with axial strain at different S_r. It can be noted that the secant modulus is

Fig. 12 Influence of S_r on the response of silty-sand subjected to UCS tests **a** stress–strain response, **b** strain-dependent secant modulus

Fig. 13 Strain-dependent dynamic properties of cohesionless BS soil obtained from Resonant Column and Cyclic Triaxial tests **a** Modulus reduction curve, **b** Damping ratio curve (Dammala et al. [8], Kumar et al. [9])

significantly affected by saturation level up to an axial strain of nearly 3%, beyond which the effect is negligible.

Dynamic properties of soils

Cohesionless BS soil

Dynamic properties such as shear modulus reduction (G/G_{max}) and damping ratio (D) of cohesionless BS soil are presented in Fig. 13. The cohesionless soil specimens were tested utilizing resonant column and cyclic triaxial tests as described by Dammala et al. [8] and Kumar et al. [9], respectively. Figure 13a presents the variations of G/G_{max} with shear strain at different range of relative density ($D_r = 30\%–90\%$) and confining pressure ($\sigma'_c = 50–300$ kPa). G/G_{max} represents the modulus reduction ratio where G represents the secant modulus while G_{max} represents the maximum shear modulus (or low-strain shear modulus). Due to the limitation of testing range of the instruments, neither the resonant column tests nor the cyclic triaxial tests can singularly provide the dynamic properties of wide shear strain ($\gamma = 10^{-4}$ %–10%). Hence, the strain-dependent shear modulus reduction (G/G_{max}) curve and damping ratio (D) curve for the wide strain range ($\gamma = 10^{-4}$–5%) is obtained by merging the curves obtained from two different testing instruments, as shown in presented in Fig. 13a
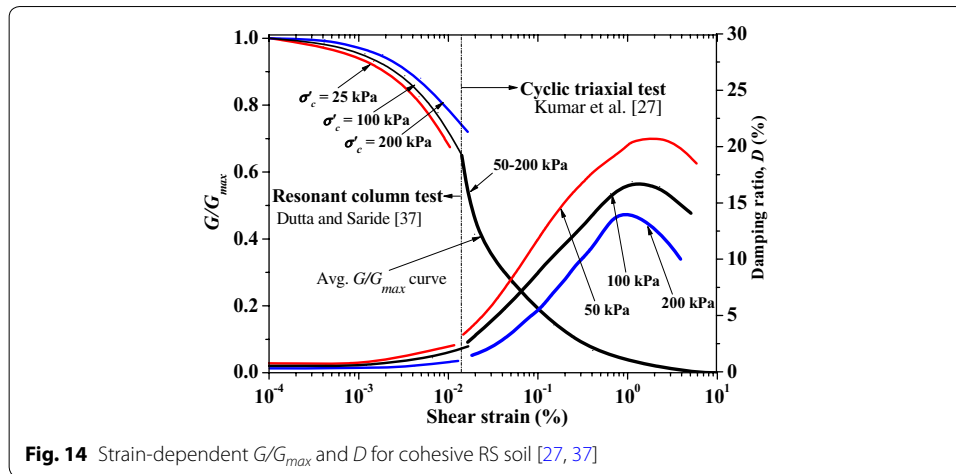
**Fig. 14** Strain-dependent G/G_{max} and D for cohesive RS soil [27, 37]

and b, respectively. The dynamic response of this soil can largely be used by the geotechnical engineers for seismic GRA and seismic soil-structure interaction for the Northeast region of India.

Cohesive RS soil

Figure 14 presents the shear modulus reduction and damping ratio of cohesive RS soil of Northeast India. The background details of the results presented in this plot is presented by Kumar et al. [27]. Thian and Lee [36] have reported that the cyclic behavior of saturated clay under undrained conditions is of utmost importance for stability of geotechnical engineering structures. Therefore, to define the dynamic properties of cohesive soil for a wide range of shear strain (i.e. from 10^{-4} to 10%), the outcomes of low strain test on similar soil [37] are also utilised in Fig. 14. Dutta and Saride [37] have performed resonant column tests on the cohesive soil, whose particle gradations were similar to the cohesive soil used in the present study. It is very difficult for geotechnical engineers and seismic analysts to find comprehensive literature on the dynamic properties of cohesive soil from Northeast region of India. Hence, the presented outcomes would aid in GRA studies for the region.

Silty-sand SS soil

To evaluate the dynamic properties of silty-sand, cyclic triaxial tests were conducted on specimens prepared at MDD-OMC and subjected to different σ'_c (50, 100 and 200 kPa) using a harmonic frequency 1 Hz. The results are presented in Fig. 15 in terms of the variations in shear modulus, G/G_{max} and damping ratio. Figure 15a presents the variations in shear modulus (G) at different σ'_c, which reflects that G increases with the increase in σ'_c. In most of the dynamic or seismic geotechnical engineering applications, G/G_{max} curve is the essential required input parameters. Hence, Fig. 15b shows the variations in normalised shear modulus (G/G_{max}) with shear strain, thereby providing the modulus reduction curve for SS soil. It is worth mentioning that there are no literature that provide the low-strain shear modulus of silty-sands of northeast region of India. Hence,
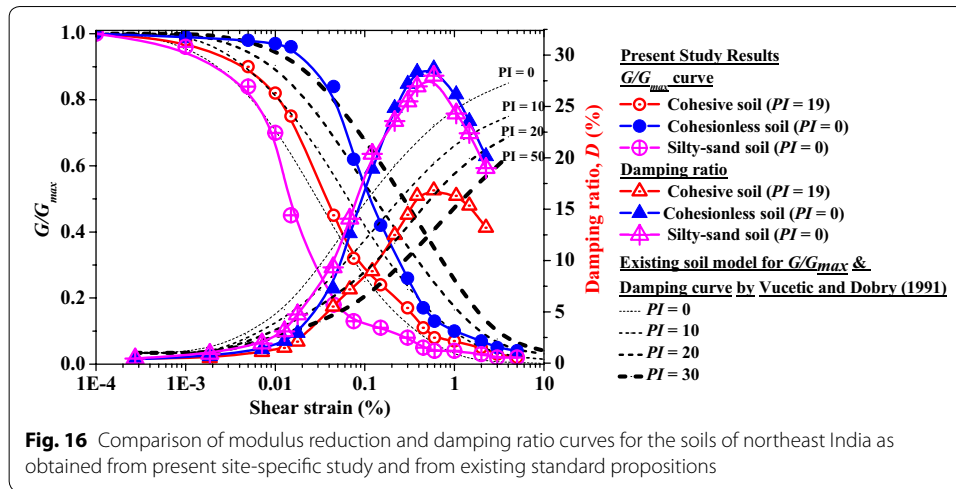
Fig. 15 Strain-dependent dynamic properties of silty-sand **a** *G*, **b** *G/G*$_{max}$ and **c** *D*
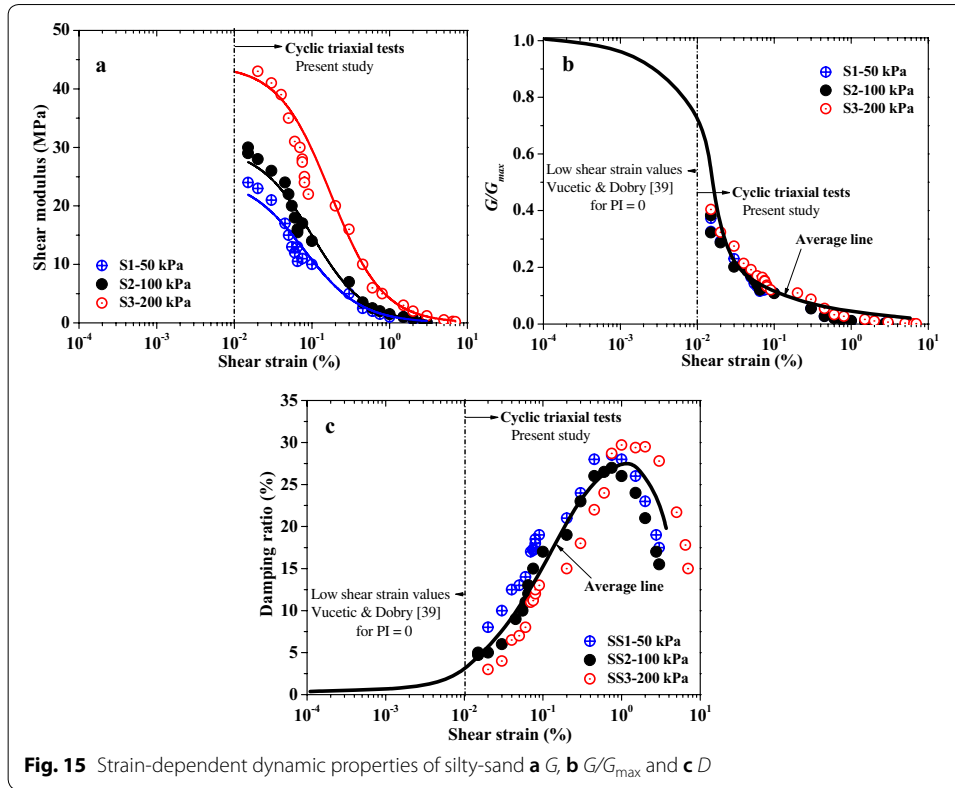
for the present context, the G_{max} of silty-sand, at different σ'_c, was evaluated using the proposition by Hardin and Drnevich [38], which is expressed as

$$G_{max} = 102132.648 \frac{(2.973 - e)^2}{(1 + e)} (OCR)^K (\sigma'_c)^{0.5} \tag{1}$$

where, e is the void ratio, OCR is the overconsolidation ratio (for present study, OCR = 1), σ'_c is the effective confining pressure, wherein σ'_c and G_{max} are in N/m^2. Figure 15b reveals that the modulus reduction curve of SS soil is negligibly affected by the variation in σ'_c. Further, the low-strain (at $\gamma < 10^{-2}$%) dynamic properties of silty sand for NE region being unavailable, the data in the specified shear strain range is obtained using the proposition by Vucetic and Dobry [39] considering $PI = 0$ (as per Table 2) for the SS soil. Figure 15c presents the variations in damping ratio (D) of silty-sand specimens. It is seen that D, obtained from cyclic triaxial tests, is marginally affected by the change in σ'_c. Figure 15c also indicates that D increases with the increase in γ up to approximately 1%, beyond which a decreasing response is noted for all the cases.

In most of the commercial software packages, the dynamic response of standard cohesionless or cohesive soils are provided in-built which aid in the dynamic response of the simulated models. The commonly used standard dynamic properties are mostly based on the propositions by Seed and Idriss [40] for cohesionless soils and by Vucetic and Dobry [39] for cohesive soils. The standard modulus reduction and damping ratio curves are based on certain index properties of the soils. A comparative analysis is carried out to understand the similarity and differences in using the standard curves with those

Fig. 16 Comparison of modulus reduction and damping ratio curves for the soils of northeast India as obtained from present site-specific study and from existing standard propositions

site-specific curves obtained from the present study on soils from northeastern region of India, and the same is exhibited in Fig. 16. It can be observed that in comparison to the standard curves, the magnitudes of site-specific modulus reduction and damping ratio are mostly different, except at very low shear-strains ($\gamma < 10^{-3}$ %). A major difference can be noted in the damping characteristics beyond 1% shear strain. It can be observed that for all the soils, the site-specific studies exhibit a decrease in the damping ratio beyond 1% shear strain, while the same is found to continually increase at all levels of shear strain when the standard propositions are used. The latter is mostly observed owing to the fact that the standard propositions are based on dynamic tests mostly conducted for $\gamma \leq 1\%$, and the developed expression is used to obtain the damping characteristics beyond 1% shear strain. Hence, in this process, any phenomenal change in the dynamic response of soils beyond 1% shear strain is overlooked and is presumed for RA studies. The site-specific experimental study on the soils of northeast region conducted at shear strains beyond 1% clearly reveals a marked change from the standard hypothesis. Such differences in damping ratio can induce marked change in the seismic response of the soil and embedded structures during the GRA or SSSI studies, and can impose a relevant difference in the design considerations. The finding from the present study for the soils of northeast India, thus, aptly justifies importance of evaluating and identifying the site-specific dynamic soil properties. For all practical purposes as well as for seismic ground engineering applications, the average magnitude of the strain-dependent dynamic properties of cohesionless BS soil, cohesive RS soil and silty-sand SS soils, at $\sigma'_c = 100$ kPa, are provided in Table 3.

Conclusions

This paper presents the results obtained from monotonic and dynamic response of soils collected from Northeast region of India. The characteristic response of cohesionless BS soil, cohesive RS soil, and silty-sand SS soil are highlighted. The influences of the variations in the relevant investigating parameters (relative density, effective confining pressure, displacement loading rate, and degree of saturation) on the monotonic and

Kumar *et al. Geo-Engineering*   (2020) 11:9

Page 19 of 21

Table 3 Average of *G/G*$_{max}$ and *D* values at different *γ* for sand, cohesive soil and silty-sand

Shear strain (%)	Sandy soil		Cohesive soil		Silty-sand	
	G/G$_{max}$	*D* (%)	*G/G*$_{max}$	*D* (%)	*G/G*$_{max}$	*D* (%)
0.0001	1	0.39	1	0.48	1	0.46
0.001	0.99	0.68	0.98	0.5	0.96	0.91
0.005	0.98	1.35	0.9	1.09	0.84	1.92
0.01	0.97	2.15	0.82	1.49	0.7	3.11
0.015	0.96	2.94	0.75	2.1	0.45	4.75
0.045	0.84	7.27	0.45	5.52	0.18	9.32
0.075	0.62	12.64	0.32	7.19	0.13	14.07
0.15	0.42	18.93	0.24	8.96	0.11	20.38
0.3	0.26	24.83	0.17	12.49	0.08	23.58
0.45	0.17	27.19	0.11	14.46	0.05	25.5
0.6	0.13	28.34	0.08	16.29	0.04	26.96
1	0.1	28.68	0.07	16.83	0.04	27.99
2	0.07	26.16	0.05	16.29	0.03	24.31
3	0.05	23.55	0.03	15.34	0.02	22.39
5	0.04	20.15	0.02	13.19	0.02	19

strain-dependent dynamic properties (shear modulus, modulus reduction and damping ratio) of the soils are discussed. It is concluded that under monotonic loading, the shear stiffness of the cohesionless BS soil is predominantly influenced by initial relative density of the prepared sample than the applied confining pressure or displacement loading rate. For the cohesive RS soil subjected to monotonic loading, although the confining pressure exhibits significant influence on the stress–strain behaviour, the secant modulus remains nearly unaffected by the change in the confining pressure. On the other hand, the stress–strain response of silty-sand SS soil is significantly affected by the change in the confining pressure. Under monotonic loading, both RS and SS soils are significantly influenced by the degree of saturation of the prepared sample. From the dynamic tests, it is concluded that the strain-dependent shear modulus (*G*) increases with the increase in σ'_c while the modulus reduction ratio, *G/G*$_{max}$, is negligibly affected. The damping ratio, *D*, is found to be marginally affected by the changes in σ'_c. From the present study, it is concluded that, irrespective of the soil type and applied effective confining stress, the damping ratio decreases beyond 1% shear strain, which a major difference from the standard propositions. From the obtained results, it is concluded that site-specific studies to decipher the dynamic properties of the soil is extremely important for GRA and SSI applications in geotechnical studies in northeast India, and such site-specific dynamic characteristics can be markedly different from the characteristics obtained from standard propositions.

Kumar *et al. Geo-Engineering*   (2020) 11:9

Page 20 of 21

Author details
[1] Department of Civil Engineering, National Institute of Technology Patna, Bihar 800005, India. [2] Department of Civil Engineering, Indian Institute of Technology, Guwahati 781039, India. [3] Department of Civil and Environmental Engineering, Indian Institute of Technology, Tirupati 517506, India.

References

1. Kramer SL (1996) Geotechnical earthquake engineering. Prentice Hall, New York
2. Dammala PK, Bhattacharya S, Krishna AM, Kumar SS, Dasgupta K (2017) Scenario based seismic re-qualification of caisson supported major bridges–A case study of Saraighat bridge. Soil Dyn Earthq Engg 100:270–275
3. IS-1893 (2002) Criteria for earthquake resistant design of structures-general provisions and buildings. Bureau of Indian Standard, New Delhi
4. Khattri KN (1992) Probabilities of occurrence of great earthquakes in the Himalaya. Proc Indian of Acad Sci Earth Planet Sci 108:87–92
5. Poddar SMC (1953) A short note on the Assam earthquake of August 15, 1950. A compilation of papers on the Assam earthquake of August 15, 1950, Government of India
6. Raghukanth STG (2008) Simulation of strong ground motion during the 1950 great Assam earthquake. Pure Appl Geophy. 165:1761–1787
7. Raghukanth STG, Dash SK (2010) Evaluation of seismic soil-liquefaction at Guwahati city. Environ Earth Sci 61:355–368. https://doi.org/10.1007/s12665-009-0347-3
8. Dammala PK, Murali Krishna A, Bhattacharyya S, Nikitas G, Rouholamin M (2017) Dynamic soil properties for seismic ground response in Northeastern India. Soil Dyn Earthq Engg 100:357–370
9. Kumar SS, Krishna AM, Dey A (2017) Evaluation of dynamic properties of sandy soil at high cyclic strains. Soil Dyn Earthq Engg 99:157–167
10. Kumar SS, Krishna AM, Dey A (2018) High strain dynamic properties of perfectly dry and saturated cohesionless soil. Indian Geotech J 48(3):549–557
11. Kumar SS, Dey A, Krishna AM (2018) Importance of site-specific dynamic soil properties for seismic ground response studies: ground response analysis. Int J Geotech Earthq Engg 9(1):78–98
12. Ordonez GA (2000) A computer program for the 1D analysis of geotechnical earthquake engineering problems. SHAKE2000 Manual, pp. 266
13. Hashash YMA, Groholski DR, Phillips CA, Park D, Musgrove M (2016) DEEPSOIL version 6.0. Tutorial and user Manual, 98p
14. Brinkgreve RBJ, Kumarswamy S, Swolfs WM, Foria F (2017) PLAXIS 3D manual. 46p
15. Kumar SS, Dey A, Krishna AM (2020) Liquefaction potential assessment of Brahmaputra sand based on regular and irregular excitations using stress-controlled cyclic triaxial test. KSCE J Civ Eng. https://doi.org/10.1007/s12205-020-0216-x
16. IS: 2720: Part-4 (1975) Grain size analysis. Bureau of Indian Standards, New Delhi
17. ASTM D2487 (2011) Standard practice for classification of soils for engineering purposes (Unified Soil Classification System). ASTM International, West Conshohocken, PA. https://doi.org/10.1520/D2487-11
18. IS: 2720: Part-3 (1981) Determination of specific gravity-fine, medium and coarse grained soils. Bureau of Indian Standards, New Delhi
19. IS: 2720: Part-14 (1983) Determination of density index of cohesionless soils. Bureau of Indian Standards, New Delhi
20. ASTM D6913/D6913M (2017) Standard test methods for particle-size distribution (gradation) of soils using sieve analysis. ASTM International, West Conshohocken, PA. https://doi.org/10.1520/D6913_D6913M-17.
21. ASTM D7928 (2017) Standard test method for particle-size distribution (gradation) of fine-grained soils using the sedimentation (hydrometer) analysis, ASTM International, West Conshohocken, PA. https://doi.org/10.1520/D7928-17
22. ASTM D0854 (2014) Standard test methods for specific gravity of soil solids by water pycnometer. ASTM International, West Conshohocken, PA. https://doi.org/10.1520/D0854-14
23. ASTM D4318 (2017) Standard test methods for liquid limit, plastic limit, and plasticity index of soils, ASTM International, West Conshohocken, PA. https://doi.org/10.1520/D4318-17
24. ASTM D0698 (2012) Standard test methods for laboratory compaction characteristics of soil using standard effort (12400 ft-lbf/ft^3 (600 kN-m/m^3)). ASTM International, West Conshohocken, PA. https://doi.org/10.1520/D0698-12E02
25. ASTM D3999/D3999M (2017) Standard test methods for the determination of the modulus and damping properties of soils using the cyclic triaxial apparatus. ASTM International, West Conshohocken, PA. https://doi.org/10.1520/D3999_D3999M
26. Kumar SS, Dey A, Krishna AM (2015) Dynamic response of river-bed sands using cyclic triaxial tests. In Proc 5th Indian Young Geotech Engg Conf (5IYGEC), Badodra, 14 March 2015, Shweta Publications
27. Kumar SS, Krishna AM, Dey A (2018) Dynamic properties and liquefaction behaviour of cohesive soil of northeast india under staged cyclic loading. J Rock Mech Geotech Engg. https://doi.org/10.1016/j.jrmge.2018.04.00
28. Yoshida N (2015) Seismic ground response analysis. Springer, New York
29. Castro G (1975) Liquefaction and cyclic mobility of saturated sands. J Geotech Engg Div 101(6):551–569
30. Kramer SL, Seed HB (1988) Initiation of soil liquefaction under static loading conditions. J Geotech Engg 114(4):412–430

Kumar *et al. Geo-Engineering*   (2020) 11:9

Page 21 of 21

31. Dash HK, Sitharam TG (2011) Undrained cyclic and monotonic strength of sand-silt mixtures. J Geotech Geolog Engg 29:555–570
32. Skempton AW (1954) The pore-pressure coefficients A and B. Geotechnique 4:143–147
33. Fredlund DG, Rahardjo H (1993) Soil mechanics for unsaturated soils. Wiley, New York
34. Ishihara K (1993) Liquefaction and flow failure during earthquakes. Geotechnique 43:351–415
35. Budhu M (2008) Soil mechanics and foundations. Wiley India Pvt, Ltd
36. Thian SY, Lee CY (2017) Cyclic stress-controlled tests on offshore clay. J Rock Mech Geotech Engg 9:376–381
37. Dutta TT, Saride S (2015) Dynamic properties of compacted cohesive soil based on resonant column studies. Int Conf Geo-Engg Climate Change Technologies for Sustainable Environ Manag, MNNIT Allahabad, pp 1–6
38. Hardin BO, Drnevich VP (1972) Shear modulus and damping in soils: design equations and curves. J Soil Mecha Found Div 98:667–692
39. Vucetic M, Dobry R (1991) Effect of soil plasticity on cyclic response. J Geotech Engg 117:89–107
40. Seed HB, Idriss IM (1970) Soil moduli and damping factors for dynamic response analysis. Report EERC 70:10

Publisher's Note

Springer Nature remains neutral with regard to jurisdictional claims in published maps and institutional affiliations.